Intracavity Optical Trapping with Ytterbium Doped Fiber Ring Laser

R. Sayed[1–2], F. Kalantarifard[3], P. Elahi[3], F. Omer Ilday[3], G. Volpe[3], O. M. Maragò[2]

[1] *Dottorato in Fisica dell' Università di Messina, Dip.to di Fisica, F. S. D'Alcontres, 98166 S. Agata, Messina, Italy*
[2] *CNR-IPCF, Istituto per i Processi Chimico-Fisici, 1-98158 Messina, Italy*
[3] *Department of Physics, Bilkent University, 06800 Ankara, Turkey.*

E-mail: rania_ sayed80@yahoo.com

Abstract

We propose a novel approach for trapping micron-sized particles and living cells based on optical feedback. This approach is implemented at low numerical aperture (NA=0.5, 20X) and long working distance. In this configuration, an optical tweezers is constructed inside a ring cavity Fiber laser and the optical feedback in the ring cavity is controlled by the light scattered from a trapped particle.

Keywords: Optical trapping, fiber ring laser, optical feedback, particle tracking, video microscopy.

Introduction

Arthur Ashkin pioneered the field of laser-based optical trapping in the early 1970s. He developed a stable, three-dimensional trap based on counterpropagating laser beams. This seminal work eventually led to the development of the single-beam gradient force optical trap [1] or "optical tweezers" as it has come to be known. The ability of optical tweezers to manipulate particles precisely and nondestructively has allowed a wide and growing variety of applications in different fields of sciences such as cellular and molecular biology, soft matter, nanotechnology and physics. The ability to apply forces in the range of femto to pico Newton on nanoparticles and to measure their displacements with nanometer precision is crucial for the investigation of colloidal and condensed matter systems [2]. More recently OTs have been also used to manipulate, rotate and assemble a variety of nanostructures, such as carbon nanotubes, nanowires, polymer nanofibers, and metal nanoparticles [3].

In recent years fiber lasers have made significant progress in capability, including high output power, excellent beam quality, compact size, long life time, low maintenance and operational robustness. With the improvements made in gain fiber and fiber Bragg-grating mirrors, higher powers and therefore more widespread applications are enabled. Optical feedback achieved inside a ring cavity Fiber laser not only enhances the wavelength tenability, but also reduces the intrinsic linewidth of spectral line.

In this paper, we demonstrate a novel technique for optical tweezing by using the optical feedback inside the ring cavity fiber laser [4]. In standard OT high intensity of the laser in the focal spot is often undesirable because of possible photodamage of the trapped sample. Here, the use of optical feedback in a ring cavity fiber laser reduces the intensity of operation of the trap. We demonstrate stable trapping operation employing low numerical aperture objectives (NA=0.5). In this novel experimental configuration the optical feedback on the fiber laser source is controlled by the light scattering from the trapped particle. When there is no particle in the trap, the optical feedback increases the trapping power in the focal point above the microscope objective. Instead, when a particle falls in the trap the optical feedback is reduced and the trap works at low powerpreventing photodamage and relaxing the stringent conditions on high numerical aperture for standard optical tweezers (typically NA 1.3).

Theory and overview

Ring fiber lasers have the ability to provide stable, single-frequency, and extremely narrow-linewidth laser oscillation. The two most important parameters characterizing a laser are the threshold pump power and the efficiency with which the laser converts the pump power into laser power once it has reached threshold. Laser threshold is determined by requiring that the gain compensate total cavity losses during each round trip [5–7] . If we consider a Fabry-Perot cavity, formed by placing two mirrors of reflectivities R1 and R2 at the two ends of a fiber of length L, in case fiber ring laser R1 and R2 represent the reflectivity of fiber Bragg Grating (FBG) of gain fiber , the threshold condition becomes

$$G^2 R_1 R_2 exp(-2\alpha_{int} L) = 1 \qquad (1)$$

where G is the single pass amplification factor and α_{int} accounts for internal losses within the cavity.

The single-pass amplification factor should include the nonuniform nature of the gain coefficient. The threshold condition is given by:

$$\alpha_{mir} + \alpha_{int} = \alpha_{cav} \tag{2}$$

where $\alpha_{mir} = -ln\frac{R_1 R_2}{2L}$ is the effective mirror loss and α_{cav} is the total cavity loss. Below or near laser threshold, gain saturation can be neglected and a fraction of intracavity power P_s is transmitted from each mirror as the output power. The pump power needed to reach threshold is thus given by:

$$P_p(0) = \frac{\alpha_{cav} L}{1 - exp(-\alpha_p L)} \left(\frac{\alpha_p}{\alpha_s}\right) P_p^{sat} \tag{3}$$

where α_p and α_s are the absorption coefficients at the pump and signal wavelengths, respectively. This expression shows how the laser threshold depends on the cavity length. It is common to write the threshold power in terms of the absorbed pump power using

$$P_{abs} = P_p(0)\,[1 - exp(-\alpha_p L] \tag{4}$$

From Eqs. 3 and 4, the threshold power P_{th} is given by:

$$P_{th} = \alpha_{cav} L \left(\frac{\alpha_p}{\alpha_s}\right) P_p^{sat} \tag{5}$$

This equation shows how laser threshold depends on parameters associated with the gain medium (dopants) and the laser cavity. In most cases of practical interest, mirror reflectivities (in case Fabry Perot cavity) or Fiber Bragg gratting reflectivities (in case Ring cavity) are large enough that P_s can be treated approximately as constant and it is given by the remarkably simple expression

$$P_s = P_s^{sat} \left(\frac{P_{abs}}{P_{th}} - 1\right) \tag{6}$$

where P_{abs} is the absorbed pump power. From Eqs. 4 and 5, the output power is given by:

$$P_{out} = (1 - R_1)P_s = \eta_s(P_{abs} - P_{th}) \tag{7}$$

R_1 mirror reflectivity represents a fiber Bragg grating (FBG) reflectivity in case of fiber ring laser. This equation shows that the laser power increases linearly with the absorbed pump power (in our case it is the output power of diode laser which bump fiber ring laser). The slope efficiency η_s is defined as the ratio of $\frac{P_{out}}{P_{abs}}$ and it is a measure of the efficiency with which the laser converts pump power into output power once it has reached threshold. It can be maximized by reducing cavity losses as much as possible.

Experimental set-up

The schematic of optical trapping system with intracavity feedback is shown in figure 1, as it can be seen, the experimental set-up comprises of a ring cavity fiber laser which the trapping components is a part of the cavity, which is the main difference of this system from conventional extra cavity optical trapping setups.

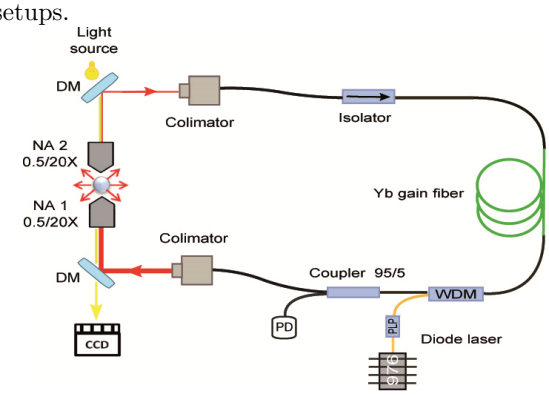

Figure 1: Sketch of the experimental set-up of optical tweezer constructed inside a ring cavity fiber laser. PLP: Pump laser protection, WDM:Wavelength division multiplexer, DM: Dichroic mirror, NA: Numerical aperture, and PD: Photodiode.

This configuration comprises of a diode-pumped Yb-fiber laser and a free space optics concerns with the trapping. The fiber laser part consists of a single mode diode laser with 976 nm center wavelength and 3 nm spectral bandwidth. The output power of diode can be increased up to 600 mw. A wavelength division multiplexer (WDM) combines the diode laser light with the fiber laser signal within the cavity at 1030 nm. The insertion loss of WDM is measured about 0.7 dB. The gain fiber is 20 cm-long single mode Yb with 500 dB gain at 976 nm. The core and clad radius of the gain fiber and other passive fibers is 6 μ m and 125 μm, respectively. An inline isolator is employed in order to make an unidirectional propagation within the cavity. By using of 5% port of a 95/5 coupler followed after isolator, the output power is monitored. A silicon photo diode convert optical signal to electrical signal is measured by an oscilloscope.

As seen from the schematic figure, one part of the cavity is free space and comprises of collimators, dichroic mirrors and objectives. The bottom collimator, collimate the output beam toward the dichroic mirror (DM). The dichroic mirror which is used in this set-up passed and reflect wavelength beyond and shorter than 1000 nm, respectively. The reflectance of the DM for 1030 nm which is the center wavelength of the laser system is measured as 90%. The reflected beam then passed through an 20X objective with 0.5 NA and focused on the sample. The diameter of the spot in the focal point is almost 2 μm. Another objective then collect the scattered beam from the particle and by using of another dichroic mirror and collimator, leads to the cavity again. Trapping of particle

by laser light increases the loss of the cavity due to scattering and as a result the threshold of laser increases and the voltage measured by the photo diode decreases.

Video particle tracking. Tracking particles in a digital video stream is a very convenient way to take position measurements, especially as most tweezers systems already feature a camera to observe the sample. Modern cameras can reach frame rates of up to tens of kHz, approaching the speeds attainable with interferometric systems. Even inexpensive cameras can now exceed 1 kHz if the acquisition region is limited to only a few trapped objects, typically a region around 50-120 pixels high and 600 pixels wide can be acquired at kHz rates on a gigabit Ethernet based camera.

The ability to use a camera simplifies taking force for two dimensional measurements. Once the magnification is known and checked with a ruled slide, camera particle tracking reads out in absolute distance units, eliminating at least one calibration step. It is also linear over the entire field of view of the camera, typically 20-100 μm. A variety of free and commercial computer programs can be used to track particles on the y with accuracy much less than a pixel, using the simple "center of mass' algorithm or other more sophisticated techniques. For microscopes used in optical tweezers, this typically results in a resolution of a few nanometers [8].

Results and discussion

Optical trapping experiments are performed in a liquid environment using calibration particles as silica and melamine microspheres with 2, 4, and 5 μm and living cells as blood, cancer and yeast as shown in figure 2. Stiffness constant (k) of trapped particle is measured at different trapping power and all measurements are carried out at room temperature.

Trapping calibration beads. A micro-particle trapped in optical tweezers is unavoidably driven by Brownian force to undertake a three-dimensional random walk around its equilibrium position within a confined volume. Under the experimental conditions reported in this paper the fluctuation of the trapped particle was found to be in the sub-micron to micron range. The particle trajectory can be conveniently tracked by CCD camer. For each particle trapped in optical tweezers with a specific set of trapping parameters (specified by optical wavelength, optical power, numerical aperture NA, etc.), optical force along each of the 2 dimensions is deduced based on the analysis of the position distribution of the particle.

In our experiments the silica bead with 4 and 5 μm are trapped at current 200 mA (power at sample is 9.7 mW). For the case of 5 μm diameter we get the trajectory of particle displacement and autocorrelation function as in figure 2. When the optical trapping power (the laser power measured at sample) is 30 mW and the numerical aperture (NA) of the focusing objective lens is 0.5 (20x), the corresponding optical force constants along the x and y directions are determined to be Kx = 0.108 $\pm$ 0.0037 pN/μm and Ky = 0.098 $\pm$ 0.0072 pN/μm . When the optical power of trapping beam increases from 9.7 mW to 42 mW the optical force becomes larger and larger as shown in figure 3(a).

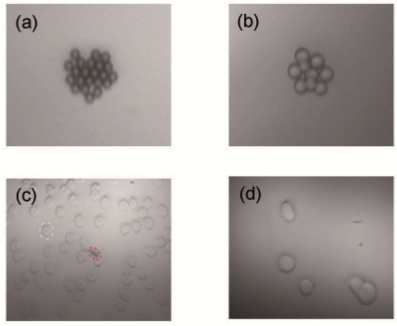

Figure 2: Trapping of particles and cells. (a) Trapping group of melamine particles with diameter 2 μm at power 22 mW. (b) Trapping group of silica particles with diameter 5 μm at power 16 mW. (c) Trapping red blood cell with diameter 8 μm at power 11 mW. (d) Trapping cancer cell with diameter 16.5 μm at power 30 mW.

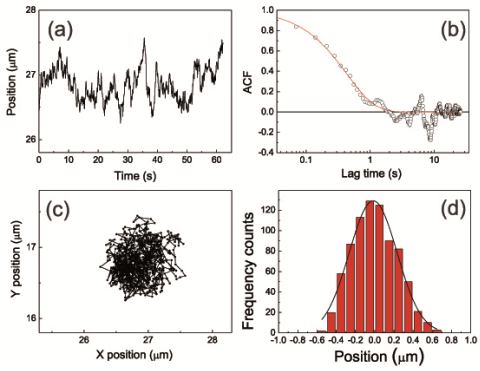

Figure 3: Calibration of optical forces on a silica bead 5 μm. (a) Fluctuations of trapped particle in X position. (b) Autocorrelation function (ACF) for trapped particle at 30 mW in x direction. (c) Trajectory of trapped particle. (d) Histogram of particle fluctuations.

Trapping living cells. Optical forces (on the order of a few pico Newtons to tens of pico Newtons) in optical tweezers with near infrared (NIR) laser beam

at 1.06 μm wavelength were soon demonstrated for non-invasive trapping and manipulation of a single living cell [9].

With proper force calibration, optical tweezers can be used as a convenient force transducer for the measurement of biological molecular interactions. When the biological cell trapped the optical force constant confining the cell can be measured by tracking and analysing it in 3 dimensions. The force constant may vary significantly from one cell to another even under the same experimental conditions. In this experiment single living cell can be trapped and analysed the two dimensional optical force field with the same method as microparticle. Under the same experimental conditions (laser wavelength 1030 nm, output power 72 mW, NA=0.5) the optical forces on the red blood cell and white blood cell are measured separately during increasing the optical power at sample from 10 mW to 42 mw as shown in figure 3(b). For sample preparation of white blood cells, fresh blood cells are suspended in a viscous fluid, Dulbecco's Modified Eagle's Medium formulation (DMEM), and Centrifugation is carried out in order to purify plasma from formed elements of the blood including platelets that can be trapped together with red blood cells (RBCs) and preventing correct measurements. The red blood cell is much more sensitive to laser light, it rotates and changes the physical shape during trapping and by increasing the trapping power to 22 mW the cell die. In contrast the white blood cell can trap at higher power without any change in the shape.

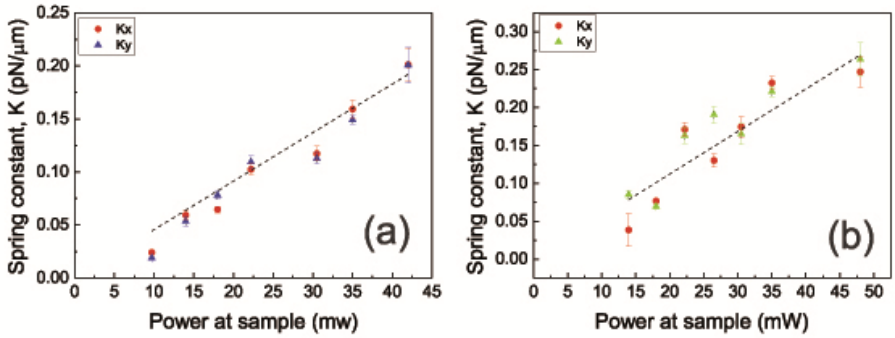

Figure 4: (a) Optical force as a function of laser power at sample for silica bead 5 μm in x and y directions. (b) Optical force as a function of laser power at sample for white blood cell 7.8 μm in x and y directions.

Conclusions

To conclude, we have provided a novel technique for optical trapping with a fiber ring laser system based on low numerical aperture objective (NA=0.5/20X). By this technique we trap calibration beads 4, 5 μm and single living cell as yeast, blood, cancer cell. Intracavity optical trapping with low numerical aperture lenses increases trapping depth, efficiency and spatial range in experiments holding promises for applications on biological systems that are affected by photodamage.

References

[1] Ashkin, A. et al.: *Observation of a Single Beam Gradient Force Trap for Dielectric Particles* ., Opt. Lett. 11, 1986, P. 288.

[2] Donato, M. G., Vasi, S., Sayed, R. et al.: *Optical Trapping of Nanotubes with Cylindrical Vector Beams.*, Opt. Lett. 37, 2012, P. 3381.

[3] Maragó, O. M. et al.: *Optical Trapping and Manipulation of Nanostructures.*, Nature Nanotech. 8, 2013, P. 807.

[4] Sayed, R. et al.: *Intracavity Optical Trapping with Ytterbium Doped Fiber Ring Laser.*, SPIE Proceedings. 8810, 2013, P. ....

[5] Svelto, O. : *Principles of Lasers*, 4th ed. Plenum, New York, 1998, P. 3381.

[6] Hanna, D. C. et al.: *Frequency upconversion in Tm and Yb-Tm Doped Silica Fibers*, Opt. Commun. 78, 1990, P. 187.

[7] Allain,Y. J. et al: *Tunable CW lasing around 610, 635, 695, 715, 885 and 910 nm in Praseodymium-doped Uorozirconate Fibre*, Electron. Lett. 27, 1991, P. 189.

[8] Bowman, R. W. and Padgett, M. G.: *Optical Trapping and Binding*, Rep. Prog. Phys. 76, 2013, P. 1.

[9] Ashkin, A. and Dziedzic, J. M.: *Optical Trapping and Manipulation of Single Cell Using Infrared Laser Beam.*, Nature 330, 1987, P. 769.

Spontaneous Casimir Effect

R. Stassi[1], S. Savasta[1]

[1] *Dipartimento di Fisica e Scienze della Terra, Università di Messina, Italy*

E-mail: rstassi@unime.it

Abstract

One of the most surprising predictions of modern quantum theory is that the vacuum of space is not empty but filled with a *sea* of virtual particles. These short-lived fluctuations are the origin of some of the most important physical processes in the universe. A quite direct evidence of the existence of such virtual particles is provided by the dynamical Casimir effect. It predicts that rapid modulations of the boundary conditions of a quantum field induce vacuum amplification effects that result in the creation of real particles out of vacuum fluctuations. Here we show that a spontaneous release of virtual photons from the quantum vacuum can occur in a quantum optical system in the ultrastrong coupling regime. In this regime, which is attracting interest both in semiconductor and superconducting systems, the light-matter coupling rate $\Omega_{\rm R}$ becomes comparable to the bare resonance frequency of photons ω_0. In contrast to the dynamical Casimir effect and other pair creation mechanisms, this phenomenon does not require external forces or time dependent parameters in the Hamiltonian. It resembles the production of particles during the early universe expansion induced by the decay of a false vacuum according to inflationary cosmology.

Keywords: Casimir effect, ultrastrong coupling regime, light-matter interaction.

Introduction

The dynamical Casimir effect has been recently experimentally realized in a superconducting circuit by modulating the inductance of a quantum interference device at high frequencies. Other proposed vacuum amplification mechanisms , as the Schwinger process and the Hawking radiation, require the presence of huge external fields or, as the Unruh effect, the presence of a rapidly nonuniformly accelerating observer, and still await observation. The here described spontaneous release of virtual photon pairs in the absence of any external drive or observer acceleration resembles the particle production during the universe expansion predicted by modern inflationary cosmology. According to this theory, a scalar field starting in the false vacuum state eventually decays, and the energy that had been locked in it is released to form a hot, uniform soup of particles, which is the assumed starting point of the traditional big bang theory. The Hamiltonian of a realistic atom-cavity system contains so-called counter-rotating terms allowing the simultaneous creation or annihilation of an excitation in both atom and cavity mode. These terms can be safely neglected for small coupling rates $\Omega_{\rm R}$ (rotating-wave approximation). However, when $\Omega_{\rm R}$ becomes comparable to the cavity resonance frequency of the emitter or the resonance frequency of the cavity mode, the counter-rotating terms are expected to manifest, giving rise to exciting effects in cavity QED. This ultrastrong-coupling regime is difficult to reach in quantum-optical cavity QED, but was recently realized in a variety of solid-state quantum systems. Such regime is challenging from a theoretical point of view as the total number of excitations in the cavity-emitter system is not preserved, even though its parity is. It has been shown that, in the ultrastrong coupling regime, the quantum optical master equation fails to provide the correct description of the system's interaction with reservoirs. Moreover quantum optical normal order correlation functions fail to describe photodetection experiments for such systems [1]. Specifically, for a single mode resonator, the photon rate that can be detected by a photoabsorber is no longer proportional to $\langle a^\dagger(t)a(t)\rangle$, where a and $a^\dagger$ are the photon destruction and creation operators of the cavity mode, but to $\langle X^-(t)X^+(t)\rangle$, where $X^+(t)$ is the positive frequency component of the quadrature operator $X(t) = a(t) + a^\dagger(t)$ [2]. A puzzling property of these systems is that their ground state is a squeezed vacuum containing correlated pairs of cavity photons. The photon pairs in this ground state $|\tilde{0}\rangle$ are, however, virtual and cannot be detected, as $\langle\tilde{0}|X^-(t)X^+(t)|\tilde{0}\rangle = 0$ [2]. Otherwise, an observation of a stream of photons from such a system in its ground state would give rise to *perpetuum mobile* behaviors. Nevertheless, we show [3] that such virtual photon pairs, dragged by spontaneous decay processes reaching or starting from states of the quantum emitter not coupled to the resonator, may be spontaneously released and directly observed. A detailed analysis, carried out be-

low, shows that such puzzling phenomenon is traceable to a general feature of open quantum systems: spontaneous transitions induced by a reservoir occur among eigenstates of the total Hamiltonian (environment induced superselection of energy eigenstates). Such general feature, in presence of a ground state with virtual excitations (or also excited states that are not orthogonal to the zero-excitation state), induces the spontaneous Casimir effect here presented.

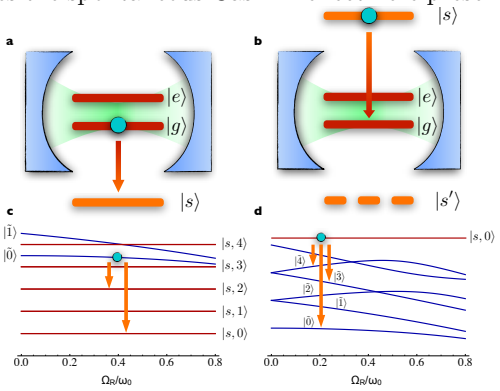

Figure 1: Sketch of the system under consideration.

The most promising candidates for an experimental realization of the proposed setting are superconducting quantum circuits and intersubband quantum well polaritons.

Theory

In the absence of losses, the quantum systems that show a spostaneous Casimir effect, depicted in Figs. 1a and 1b, are described by the total Hamiltonian H,

$$H = \omega_0 a^\dagger a + \sum_{\alpha=\mathrm{s,g,e}} \omega_\alpha \sigma_{\alpha\alpha} + \Omega_\mathrm{R}(a + a^\dagger)(\sigma_\mathrm{eg} + \sigma_\mathrm{ge}) \,, \tag{1}$$

where ω_0 is the frequency of the cavity mode, ω_α ($\alpha = \mathrm{s,g,e}$) are the bare frequencies of the atomic-like relevant states, and $\sigma_{\alpha\beta} = |\alpha\rangle\langle\beta|$ describes the transition operators (projection operators if $\alpha = \beta$) involving the levels of the quantum emitter. It is useful to label with $|j\rangle$ (j integer) the eigenstates of H, and with Ω_j (increasing with j) the corresponding eigenenergies. The Hamiltonian H describes a cascade three-level system with only one transition $|\mathrm{g}\rangle \leftrightarrow |\mathrm{e}\rangle$ resonantly coupled with a single mode of an optical resonator. Hence, when the system is in the state $|\mathrm{s}\rangle$, it does not interact with the resonator. The Hamiltonian can be split up as $H = H_\mathrm{Rabi} + H_S$, where H_Rabi is the well known Rabi Hamiltonian and $H_\mathrm{s} = \omega_\mathrm{s}\sigma_\mathrm{ss}$. As a consequence the total Hamiltonian is block-diagonal and its eigenstates can be separated into (i) a non-interacting sector $|\mathrm{s}, n\rangle$, with energy $\omega_\mathrm{s} + n\omega_0$, where n labels the cavity photon number; and into (ii) dressed atom-cavity states $|\tilde{j}\rangle$, resulting from the diagonalization of the Rabi Hamiltonian H_Rabi. Panels c and d in Fig. 1 display the lowest energy levels (resulting from the numerical diagonalization of H) for the two configurations shown in panels a and b respectively as a function of the normalized coupling $\Omega_\mathrm{R}/\omega_0$. The equally energy-spaced flat lines (red) correspond to eigenstates of the non-interacting sectors $|\mathrm{s}, n\rangle$. The energy levels (blue) that split and then bend as a function of the $\Omega_\mathrm{R}/\omega_0$ correspond to the eigenvectors $|\tilde{j}\rangle$. The ground state of this sector can be expanded in terms of the bare photon and emitter states as

$$|\tilde{0}\rangle = \sum_{k=0}^{\infty} (c^{\tilde{0}}_{\mathrm{g},2k}|\mathrm{g}, 2k\rangle + c^{\tilde{0}}_{\mathrm{e},2k+1}|\mathrm{e}, 2k+1\rangle) \,. \tag{2}$$

In the intermediate regime, where $\Omega_\mathbf{R}$ is small compared to $\Sigma = \omega_0 + \omega_\mathrm{eg}$ (where $\omega_{\alpha\beta} = \omega_\alpha - \omega_\beta$), an approximate simple analytical form of the energy spectrum and the eigenstates can be derived. Within this approximation, the dressed ground state reduces to

$$|\tilde{0}\rangle \simeq c^{\tilde{0}}_{\mathrm{g},0}|\mathrm{g}, 0\rangle + c^{\tilde{0}}_{\mathrm{g},2}|\mathrm{g}, 2\rangle + c^{\tilde{0}}_{\mathrm{e},1}|\mathrm{e}, 1\rangle \,, \tag{3}$$

where $c^{\tilde{0}}_{\mathrm{e},1} \simeq \Omega_\mathrm{R}/\Sigma$ and $c^{\tilde{0}}_{\mathrm{g},2} \simeq \Omega_\mathrm{R}^2/(\sqrt{2}\omega_0\Sigma)$. For $\Omega_\mathrm{R}/\omega_0 \ll 1$, the Jaynes-Cummings (JC) model is recovered and only $c^{\tilde{0}}_{\mathrm{g},0} \neq 0$. For larger couplings, e.g. $\Omega_\mathrm{R}/\omega_0 0.1$, the two excitation amplitudes $c^{\tilde{0}}_{\mathrm{g},2}$ and $c^{\tilde{0}}_{\mathrm{e},1}$ become non-negligible. Analogously the excited states can be expanded as

$$|\tilde{j}\rangle = \sum_{k=0}^{\infty} (c^{\tilde{j}}_{\mathrm{g},k}|\mathrm{g}, k\rangle + c^{\tilde{j}}_{\mathrm{e},k}|\mathrm{e}, k\rangle) \,. \tag{4}$$

In contrast to the JC model, they are not in general orthogonal to $|\mathrm{g}, 0\rangle$ (being $c^{\tilde{j}}_{\mathrm{g},0} \neq 0$), hence they can have a nonzero probability to have zero bare excitations. All subsequent calculations are performed at zero detuning: $\omega_0 = \omega_\mathrm{eg}$.

In the first of the two configurations (see Fig. 1a,c) that we consider, the system is initially prepared, e.g. by adiabatic excitation (slow as compared with the inverse of Ω_R), in the lowest energy dressed state $|\tilde{0}\rangle$. Although in the ultrastrong coupling regime this state contains virtual cavity photons ($\langle\tilde{0}|a^\dagger a|\tilde{0}\rangle \neq 0$), it is a vacuum state for the physical cavity photons that can be detected: $X^+|\tilde{0}\rangle = 0$ and hence $\langle\tilde{0}|X^- X^+|\tilde{0}\rangle = 0$. Since $|\tilde{0}\rangle$ is not the lowest energy vacuum, it can be considered as the photonic false vacuum, since in this case the state $|\mathrm{s}, n = 0\rangle$ is the lowest energy (true) vacuum state. Interesting theoretical studies of quantum dynamics in these cavity QED systems with [4, 5] and without the rotating-wave approximation recently appeared. Panel 1c displays the lowest energy levels (the eigenvalues of H: $\omega_\mathrm{s} + n\omega_0$ and $\omega_{\tilde{j}}$) as a function of Ω_R. Let us discuss the spontaneous decay of the initial state $|\mathrm{I_a}\rangle = |\tilde{0}\rangle$, keeping in mind that spontaneous transitions induced by a reservoir occur among

eigenstates of the total Hamiltonian (environment induced superselection of energy eigenstates). For zero or small coupling rates $\Omega_{\rm R}$, the initial state $|\tilde{0}\rangle$ reduces to $|{\rm g},0\rangle$ and standard spontaneous emission of a photon (at energy $\omega_{\rm gs}$) in the external electromagnetic modes, associated with the emitter transition $|{\rm g}\rangle$–$\sigma_{\rm sg}|{\rm g}\rangle = |{\rm s}\rangle$, occurs at a rate $\gamma_{\rm gs}$ (fixed by the dipole moment of the transition). In the ultrastrong coupling regime, the initial state is $|{\rm I_a}\rangle = |\tilde{0}\rangle$ and possible final states are $|{\rm F}_i\rangle = |{\rm s}, 2i\rangle$, with transition amplitude $\propto \langle {\rm F}_i|\sigma_{\rm sg}|{\rm I_a}\rangle = c^{\tilde{0}}_{{\rm g},2i}$. Of course spontaneous transitions occurs only if the final states have lower energy than the initial one ($\omega_{\rm s} + 2i\omega_0 < \omega_{\tilde{0}}$). For $i = 0$, the final state contains no cavity photons as in ordinary spontaneous emission. For coupling rates $\Omega_{\rm R}/\omega_0 < 1$, the contribution with $i = 1$ provides the next dominant term. Hence the spontaneous emission of a photon not in the cavity mode at a rate $\gamma_{\rm gs}$ comes together with a flux of cavity photon pairs at a rate $\approx \gamma_{\rm gs}|c^{\tilde{0}}_{{\rm g},2}|^2$.

In the second configuration, shown in Fig. 1b, the system is initially prepared into the cavity-uncoupled level $|{\rm I_b}\rangle = |{\rm s},0\rangle$, which is at higher energy with respect to state $|{\rm e}\rangle$. In this case, the initial state can be prepared exciting the matter system from a ground state $|{\rm s}'\rangle$, without involving the emitter states coupled with the resonator. However such setting works even in the absence of $|{\rm s}'\rangle$. We consider the case where spontaneous emission induces the following transition: $|{\rm s}\rangle$–$|{\rm g}\rangle$, as the transition $|{\rm s}\rangle$–$|{\rm e}\rangle$ is forbidden. For small coupling rates $\Omega_{\rm R}/\omega_0 \ll 1$, standard spontaneous emission of a photon at energy $\omega_{\rm sg}$ directly in the external electromagnetic modes at a rate $\gamma_{\rm sg}$ would be observed. In the ultrastrong coupling regime possible final states are $|{\rm F}_{\tilde{j}}\rangle = |\tilde{j}\rangle$, where $\langle {\rm F}_{\tilde{j}}|\sigma_{\rm gs}|{\rm I_b}\rangle = c^{\tilde{j}}_{{\rm g},0}$. The coefficient $c^{\tilde{j}}_{{\rm g},0}$ describes the probability amplitude that the state $|\tilde{j}\rangle$ has zero cavity photons. For negligible couplings, only $c^{\tilde{0}}_{{\rm g},0} \neq 0$, thus the only possible final state would be $|\tilde{0}\rangle$. In this case no cavity photons would be observed, since $\langle\tilde{0}|X^-X^+|\tilde{0}\rangle = 0$. In the ultrastrong coupling regime, $c^{\tilde{j}}_{{\rm g},0} \neq 0$ for even excited states (with the same parity as $|{\rm g},0\rangle$), hence spontaneous transitions $|{\rm s},0\rangle$–$|{\rm F}_{\tilde{j}}\rangle$ can occur even for $\tilde{j} \neq \tilde{0}$. In particular, the next largest coefficients are those for $\tilde{j} = 3, 4$. These excited dressed states emit physical photon pairs ($\langle\tilde{3}|X^-X^+|\tilde{3}\rangle \neq 0$). It is amazing and counterintuitive that cavity photon-pairs are emitted only because there are excited states of the cavity-matter system which have a nonzero probability of having zero cavity photons!

Results

For describing a realistic system, the cavity and atom dissipation channels need to be taken into account. Yet, owing to the very high ratio $\Omega_{\rm R}/\omega_0$, the description offered by the standard quantum optical master equation can break down, for example producing spurious qubit flipping or photon generation, even at zero temperature. Following Refs., we write the Hamiltonian in a basis formed by the eigenstates of H to describe the dissipative processes. We choose a $T = 0$ temperature environment. Yet generalization to $T \neq 0$ environments is straightforward. We thus arrive at the master equation [4], $\dot{\rho}(t) = i[\rho(t), H] + \sum_c \mathcal{L}_c\rho(t)$, where $\mathcal{L}_c$ is a Liouvillian superoperator describing the cavity ($c = 0$) and the material system losses $c =$ e–g, and g–s (configuration a) or s–g (b) (see Methods for details).

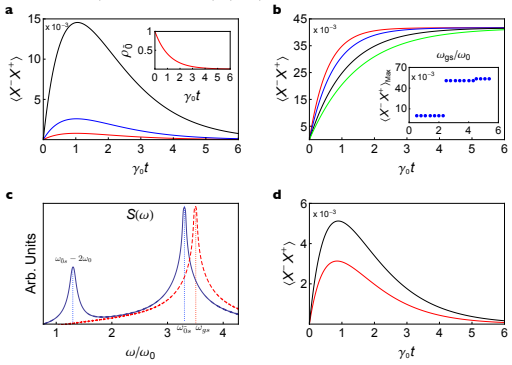

Figure 2: Dynamics of released photons and spontaneous emission spectra. a: Time evolution of the intracavity mean photon number. b: $\langle X^-X^+\rangle$ for different spontaneous emission decay rates $\gamma_{\rm gs}$ (see text) obtained by artificially dropping cavity losses. c: Spectrum $S(\omega)$ of spontaneously emitted photons. d: Time evolution of $\langle X^-X^+\rangle$ for the configuration (b) sketched in Fig. 1b.

According to the input-output relations, the destruction operator for the output field escaping a single port resonator can be espressed as $a_{\rm out}(t) = a_{\rm in}(t) - \sqrt{\gamma_0}\,X^+(t)$. The output cavity photon rate which can be detected in photodetection experiments is given by the mean value $\Phi_{\rm out} = \langle a^\dagger_{\rm out}a_{\rm out}\rangle$. If the input is in the vacuum state as in the present case, $\Phi_{\rm out}(t) = \gamma_0\langle X^-(t)\,X^+(t)\rangle$. In circuit QED systems, a particularly well suited technology for observing the spontaneous Casimir effect (Methods), this normal order correlation function can be measured by using quadrature amplitude detectors. The results of a full numerical demonstration including the cavity and the emitter losses is shown in Fig. 2. Figure 2a displays the numerically calculated time evolution of the mean cavity number of physical photons $\langle X^-(t)X^+(t)\rangle = {\rm Tr}[X^-X^+\,\rho(t)]$ for configuration (a) (see Fig. 1a and c) and for different coupling strengths $\Omega_{\rm R}/\omega_0 = 0.3$ (red line), 0.4 (blue), 0.6 (black). Calculations have been performed at zero detuning and by using $\gamma_{\rm eg} = \gamma_0 = \gamma_{\rm gs} = 2\times10^{-2}\omega_0$, $\omega_{\rm gs} = 3.5\omega_0$. The system is initially prepared in the

electrodynamics vacuum state (the false vacuum) $|\tilde{0}\rangle$. Then the spontaneous decay of such state produces an output stream of cavity photons: the unlocked virtual photons that can now be detected. Such photon stream is the signature of the spontaneous Casimir effect. The signal rapidly grows and reaches a maximum value before decaying exponentially due to cavity losses. As expected from the previous analysis, the signal increases with increasing $\Omega_{\rm R}/\omega_0$, as a consequence of the buildup of $c^{\tilde{0}}_{{\rm g},2}$. Considering a produced maximum photon number $\langle X^- X^+\rangle \approx 10^{-2}$ (see Fig. 2a) and $\gamma_0 = 2\times 10^{-2}\omega_0$ with $\omega_0 = 10$ GHz, the spontanous Casimir effect will give rise to a peak output photon flux $\Phi^{\rm peak}_{\rm out} \approx 1\times 10^7$ photons per second. Such a photon rate corresponds to a quite low emission power $\hbar\omega_0\ \Phi^{\rm peak}_{\rm out}$ which however can be detected with existing technology. We also notice that, for a typical system temperature $T = 20$ mK, the cavity mode energy $\omega_0 \approx 10$ GHz is much larger than KT (where K is the Boltzmann constant) and as a consequence the spontaneous Casimir photon flux is much higher than that arising from the thermal occupation of the resonator. In the absence of ultrastrong coupling ($\Omega_{\rm R}/\omega_0 \ll 1$) or dropping the counter-rotating terms in the Hamiltonian [1] would result into $\Phi_{\rm out} = 0$. The detection of a photon flux escaping the cavity is the main signature of the Spontaneous Casimir effect. Panel 2b shows calculations of $\langle X^- X^+\rangle$ for different spontaneous emission decay rates ($\gamma_{\rm gs}/\omega_0 = 10^{-2}$ (green curve), 1.5×10^{-2} (black), 3×10^{-2} (blue), 4×10^{-2} (red)) obtained by artificially dropping cavity losses ($\gamma_0 = 0$). We also used a coupling rate $\Omega_{\rm R}/\omega_0 = 0.6$ and $\gamma_{\rm eg} = \gamma_{\rm gs} = 2\times 10^{-2}\omega_0$. In the absence of cavity losses, the mean photon number reaches a maximum value which does not depend on $\gamma_{\rm gs}$. This result puts forward that the phenomenon here investigated is intrinsically different from the dynamical Casimir effect where the emitted photon rate depends strongly on the modulation frequency. The inset in Fig. 2b displays the maximum cavity mean photon number $\langle X^- X^+\rangle_{\rm Max}$ as a function of the energy difference $\omega_{\rm gs}$ obtained using $\Omega_{\rm R}/\omega_0 = 0.8$ (other parameters are the same as those used for Fig. 2a). Photon pairs are released only when $\omega_{\tilde{0}} > \omega_{\rm s} + 2\omega_0$ because the spontaneous transition $|\tilde{0}\rangle$–$|{\rm s},2\rangle$ occurs only when the energy of the final state is below that of the initial state (see Fig. 1c). Increasing $\omega_{\rm gs}$, a second rung corresponding to a small increase of $\langle X^- X^+\rangle_{\rm Max}$ can be observed. It comes from the activation of the transition $|\tilde{0}\rangle$–$|{\rm s},4\rangle$. In the dynamical Casimir effect, the energy of radiated photons comes at the expense of the mechanical energy of the moving mirror, which then experiences a friction force by the quantum vacuum via the so-called back-reaction effect. In analogy we show that the release of virtual photon pairs, present in the photonic false vacuum $|\tilde{0}\rangle$, satisfies energy conservation. The energy of the radiated cavity photons, induced by the spontaneous decay of the false vacuum, comes at the expense of the energy of the quanta emitted into the reservoir (e.g. the spontaneously emitted photons in the external electromagnetic modes). In the present case, back-reaction effects can be investigated by calculating the emission spectrum of spontaneously emitted photons directly in the external electromagnetic modes: $S(\omega) = 1/(2\pi)\int_{-\infty}^{\infty} dt \int_{-\infty}^{\infty} dt' \langle \sigma^-(t)\sigma^+(t')\rangle e^{-i\omega(t-t')}$, where $\sigma^{\pm}$ are the frequency positive (negative) components of the polarization operator $\sigma_{gs} + \sigma_{sg}$. The spectrum $S(\omega)$ of spontaneously emitted photons, calculated for $\Omega_{\rm R}/\omega_0 = 0.6$ (other parameters are the same as those used for Fig. 2a), is displayed in Fig. 2c. In the absence of interaction (dashed line), the spectrum consists of a single Lorentzian peak centered at energy $\omega_{\rm gs}$, corresponding to ordinary spontaneous emission. In the ultrastrong coupling regime the main peak is red-shifted at energy $\omega_{\tilde{0}{\rm s}}$ and a second peak at lower energy, centered at $\omega_{\tilde{0}{\rm s}} - 2\omega_0$ (see Fig. 1c) appears. This peak shows that pair creation is associated to the spontaneous emission of an outside photon of lower energy $\omega_{\tilde{0},s} - 2\omega_0$. The observation of the lower peak in the spontaneous emission spectrum of the emitter would be an additional signature of the spontaneous Casimir effect. The higher peak at energy $\omega_{\tilde{0},s}$ origins from events where pair creation is absent.

References

[1] Savasta, S. & Girlanda, R. Quantum description of the input and output electromagnetic fields in a polarizable confined system. *Phys. Rev. A* **53**, 2716–2726 (1996).

[2] Ridolfo, A., Leib, M., Savasta, S. & Hartmann, M. J. Photon blockade in the ultrastrong coupling regime. *Phys. Rev. Lett.* **109**, 193602 (2012).

[3] Stassi, R. & Ridolfo, A. & Di Stefano, O. & Hartmann, M. J. Savasta, S. Spontaneous conversion from virtual to real photons. *Phys. Rev. Lett.* **74**, 033811 (2006).

[4] Ridolfo, A., Vilardi, R., Di Stefano, O., Portolan, S. & Savasta, S. All optical switch of vacuum rabi oscillations: The ultrafast quantum eraser. *Phys. Rev. Lett.* **106**, 013601 (2011).

[5] Stassi, R., Ridolfo, A., Savasta, S., Girlanda, R. & Di Stefano, O. Delayed-choice quantum control of light-matter interaction. *EPL* **99**, 24003 (2012).